Numerical and experimental investigation of the shockwave boundary layer interaction of laminar/transitional flow past a sharp fin

T. Ecker⋆, J. Martinez Schramm⋆, L. Schmidt⋆, D. Surujhlal⋆, A. Wagner⋆ and Tim Horchler⋆
German Aerospace Center (DLR)
⋆ *Institute of Aerodynamics and Flow Technology*
Bunsenstr. 10, 37073 Göttingen, Germany
tobias.ecker@dlr.de · jan.martinez@dlr.de · leni.schmidt@dlr.de
divek.surujhlal@dlr.de · alexander.wagner@dlr.de · tim.horchler@dlr.de

Abstract

The effects of shock impingement and interference on local aerodynamic heating have been and still are a key issue for the design of hypersonic flight vehicles[1]. At this time DLR is involved in continuous series of sounding rocket flight experiments studying hot structures. One of these experiment is the STORT flight experiments[2]. One essential flown experiment is the fins experiment on the third stage. The fins were investigated both on the vehicle, in windtunnels in Cologne and Göttingen but also numerically. For the windtunnel experiment in the HEG (High Enthalpy Shock Tunnel Göttingen) the object of investigation is a plate mounted fin which scales 1:2 to the flight hardware. The fin induced shock boundary layer interaction (SBLI) on the plate leads to increased thermal loads with strong thermal gradients. The heat flux on the flat plate determined by using temperature sensitive paints (TSP[3]). In a previous study first experimental and numerical results for a sharp fin on a flat plate for two freestream HEG conditions at Mach 7.4 were presented [4]. CFD calculations at both 0 deg AoF and 15 deg AoF were performed and compared for flow topology and turbulence model influence. While the XIII condition compared well between experiment and CFD, the XV condition which showed clear signs of transitional flow exhibits rather complex physical phenomena which require further investigation, both experimentally and numerically. In the current study we extend the investigation to the other conditions/configurations studied and supplement the studies using RANS turbulence modelling by using Improved Detached eddy simulation(IDDES), as well as thermal and chemical non-equilibrium for select cases in order to gain a better understanding of the complex flow field found in the experiment.

1. Introduction

The effects of shock impingement and interference on local aerodynamic heating have been and still are a key issue for the design of hypersonic flight vehicles[1] and continue to be a programmatic inspiration for current and future work[5]. Currently DLR is involved in several flight experiments, among them CALLISTO a first stage demonstrator, REFEX which has a main focus on guidance and navigation for a gliding reentry vehicle and ATHEAT (Advanced Technologies for High Energetic Atmospheric Flight of Launcher Stages) which focuses on a hybrid upper stage. In a previous flight experiment called STORT[2, 6] (Schlüsseltechnologien für hochenergetische Rückkehrflüge von Trägerstufen / Key Technologies for High Speed Return Flights of Launcher Stages) the focus was on hot structures [7]. STORT used a three-stage sounding rocket configuration and was flying on a suppressed trajectory in order to increase integral heat load on structures [2, 8] . One essential structure flown on the STORT flight experiment is the fins experiment on the third stage. The fins were investigated both on the vehicle, in windtunnels in Cologne and Göttingen but also numerically. For the windtunnel experiment in the HEG (High Enthalpy Shock Tunnel Göttingen) the object of investigation is a plate mounted fin which scales 1:2 to the flight hardware. The fin induced shock boundary layer interaction (SWBLI) on the plate leads to increased thermal loads. The heat flux on the flat plate and fin are investigated using temperature sensitive paints (TSP[3, 9, 10]). Within the range of canonical SWBLI configurations[11] the STORT fin configuration is a special case of the fin type as it combines a sharp fin with a planar section. Deviating from the canonical shape this is more representative of flight hardware commonly found in hypersonics. Similar planar fins have been studied numerically and experimentally for fins mounted both on flat as well as cylindrical surfaces for the mean

flow topology of SWBLI by Pickles et al.[12]. Further studies on the STORT fin shape were conducted numerically and experimentally at the university of Aroizona [13, 14]. Previous proof-of-principle measurements using TSP were conducted in the AEDC wind tunnel by Smith et al[15] for a 30 deg wedge on an 33.5 deg angled plate (wedge). Based on the temperature results the authors demonstrated successful boundary layer tripping and the influence of SWBLI on surface temperatures, however the database of such studies presently in the literature is very sparse.

For the current study the flow on the plate and around the fin is studied at three experimental HEG conditions at Mach 7.4 for two fin angles (AoF). Numerical studies using RANS CFD for multiple turbulence models are performed and compared to experimental heat flux results obtained in the HEG via a TSP method.

2. Windtunnel and experimental setup

2.1 HEG

Experiments were conducted in the free-piston-driven High Enthalpy Shock Tunnel Göttingen (HEG). The HEG was commissioned and further developed in order to duplicate flight conditions for the investigation of the flow around entry and reentry vehicles during the Hermes programm. The freestream conditions pertinent to this work are representative of around 30 km altitude at Mach 7.4. The wall-to-stagnation temperature ratios were $T_w/T_0 \approx 0.1$ with stagnation enthalpies of $h_0 \approx 3.1\ MJ/kg$. Higher stagnation enthalpy test conditions are additionally available to investigate the influence of high-temperature effects such as chemical and thermal relaxation on the aerothermodynamics of entry or reentry vehicles. Further detailed information on the HEG facility is provided by Hannemann et al.´ [16]. The TSP diagnostic was used to obtain the surface heat flux distribution on the flat plate model and on the fin. The base layer was applied to the fin and a section of the flat plate on which the TSP layer was applied. Layer thickness of the TSP was estimated at approximately 3 μm. More details of TSP composition development can be found in the works of Schramm et al. and Ozawa et al. [9, 10]. For each pixel imaged from the measurement surfaces, a temporal integration of the temperature history was performed to obtain heat flux [17]. This method required an in-situ calibration of the base layer following the procedures as detailed by Schramm et al. [10] and Ozawa et al. [9]. The estimated uncertainty in the derived heat-flux was 5 % [9].

2.2 Flow conditions

The investigated flow conditions are listed in table 1. Both conditions are at M=7.4 but leverage flow conditions from laminar (XVII/XIII) to transitional/turbulent (XV) at approximately double the Reynolds number. For some cases the boundary layer (BL) is tripped in the experiment using roughness elements. For all numerical studies the wall temperature was assumed to be isothermal at 300 K.

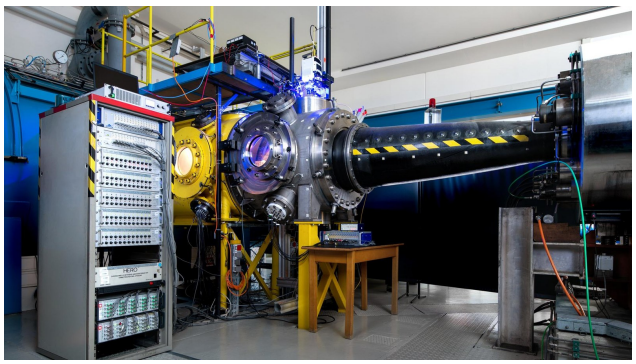

Figure 1: HEG Test section with installed nozzle. Published under CC-BY 3.0.

2.3 Fin geometry

The CAD geometry of the fin is derived from the flight geometry as communicated during the project phase. Due to the dimensions of the HEG test section the fin is scaled to 1:2 of the flight geometry. A CAD drawing of the fin geometry is shown in figure 2a. A overview of the fin plate geometry is shown in figure 2b. At zero angle of attack (called AoF: angle of fin from hereon) the fin leading edge (LE) is located 250 mm downstream from the leading edge of the flate

Table 1: HEG tunnel conditions [16].

Cond.	XVII (H3.5R2.4)	XIII (H3.3R3.7)	XV (H3.0R6.4)
M	7.4	7.4	7.3
Re_m	2.4 10^6 1/m	3.7 10^6 1/m	6.4 10^6 1/m
ρ	17.7 g/m^3	25.9 g/m^3	43.2 g/m^3
T_0	2895 K	2740 K	2582 K
flow	laminar	laminar	transitional

plate mounted in the test section. The center of rotation of the fin is located at 50% fin length. The radius of the plate LE is 0.1 mm, the length of the carrier plate is 600 mm and the width is 340 mm.

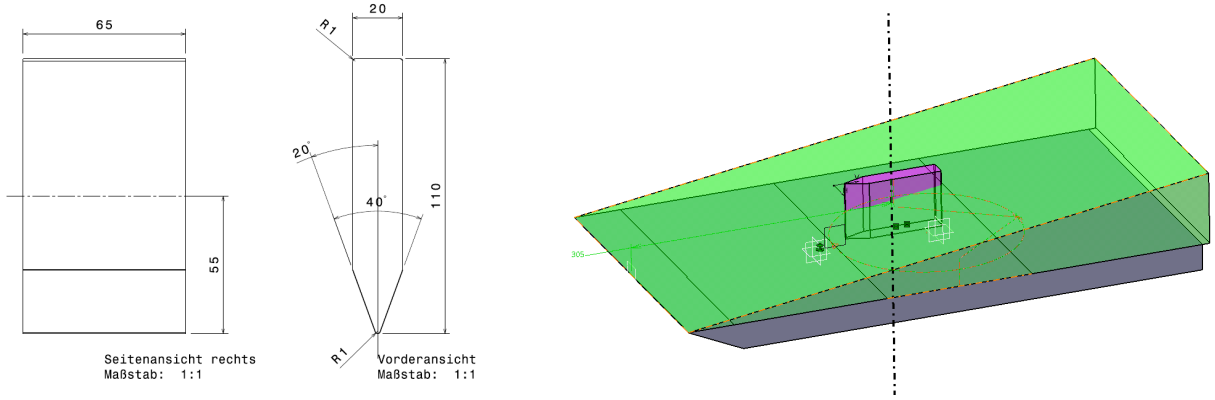

(a) Drawing of the fin geometry.

(b) CAD model, green transparent surfaces indicates shock from plate LE.

Figure 2: Experiment geometry.

2.3.1 Considered configurations

The fin on plate configuration allows to cover multiple (albeit not completely independent) flow deflection angles by turning the fin. The potential flow deflection angles are summarized in table 2. For the experimental entries only AoF of zero deg and 15 deg are available and therefore these are the cases the numerical study focuses on. For AoF of zero deg the deflection angles are symmetric at 20 deg whereas for the AoF 15 deg case both an effective 5 deg deflection and a 35 deg deflection are present.

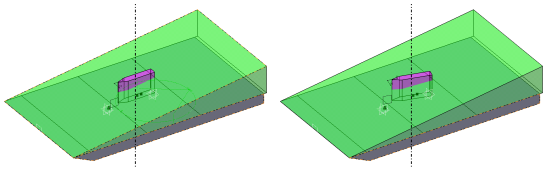

(a) 0 deg

(b) 15 deg

Figure 3: Fin angles

Table 2: Deflection matrix

AoF	angle L	angle R
0 deg	20 deg	20 deg
15 deg	5 deg	35 deg

2.3.2 Test matrix

The experimental test matrix is shown in figure 3. Two angles of attack, three windtunnel conditions and different boundary layer tripping methods were employed, resulting in seven experimental data sets. More information on the tripping methodology can be found in [18].

Table 3: Experimental matrix

ID	Cond.	AoF	roughness
1906	XIII	15 deg	no tripping, R=0.2 mm
1907		0 deg	
1908		0 deg	granular trip (1-2 mm), R=0.1 mm
1909	XV		combination granular trip (1-2 mm and 0.5-1 mm), R=0.1 mm
1910	XVII	15 deg	
1911	XV		granular trip (1-2 mm), R=0.1 mm
1912	XIII		

2.3.3 Evaluation zones

In difference to the CFD calculations, the experimental data is only available for part of the tested model due to viewing / camera limitations. Therefore comparisons are mainly made for the surfaces that are available in both datasets. The numerical domain and the experimental measurement domain are shown in figure 4 and figure 5 from a top down perspective. The different colors of the camera pixels represent different data sections from a 3D stitching process. The cone of influence drawn from the leading edge corner shows that effects from the limited span of the flat plate should be negligible. The streamwise and spanwise cuts used to extract data are shown also.

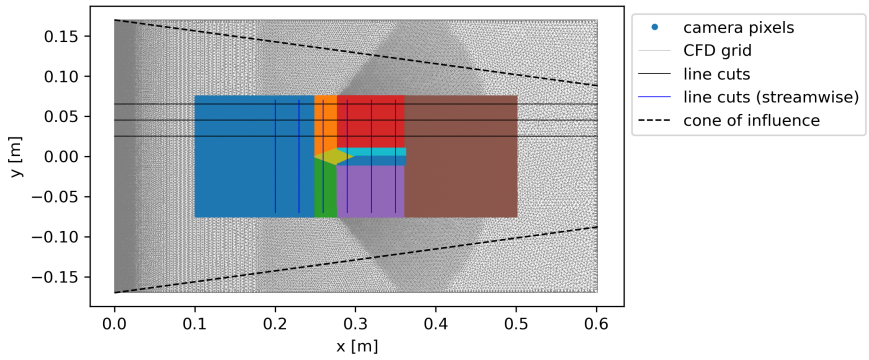

Figure 4: Top view on numerical and experimental domain - lines represent the location of data evaluation in the following analysis (y = 0.03, 0.05, 0.07 m) for the 0 deg AoF configuration.

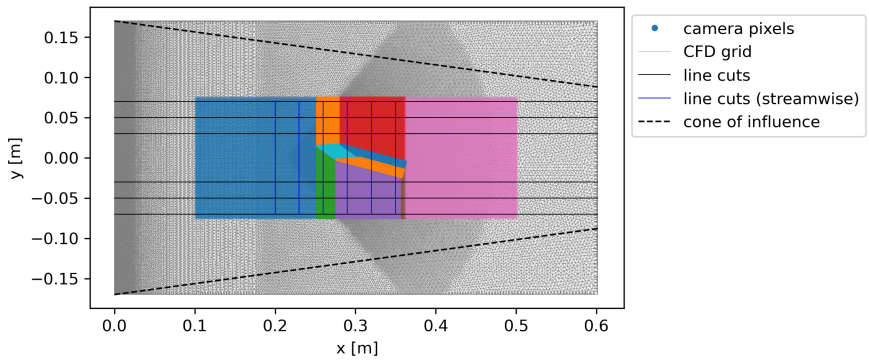

Figure 5: Top view on numerical and experimental domain - lines represent the location of data evaluation in the following analysis (y = ∓ 0.03, 0.05, 0.07 m) for the 15 deg AoF configuration.

3. Experimental results

The experimental results are grouped by the angle of fin to allow systematic comparison on the effect of tunnel condition and boundary layer tripping. A previous study[4] has elaborated on two of the presented runs and found issues with the TSP sensitivity at very high heat fluxes (or temperatures) causing essentially saturation at these locations. Further issues were found with the side view of the fin, therefore it is focused on the top view of the SBLI only. Even though issues with TSP sensitivity complicate the analysis of the peak heat flux the data is still valuable as one of the few datasets presenting the SBLI for a larger domain in the vicinity of the shock generator. The fin mounted on a plate in the HEG test section is shown in figure 6. Optical access is from the side, the top and from a 45 deg angle port.

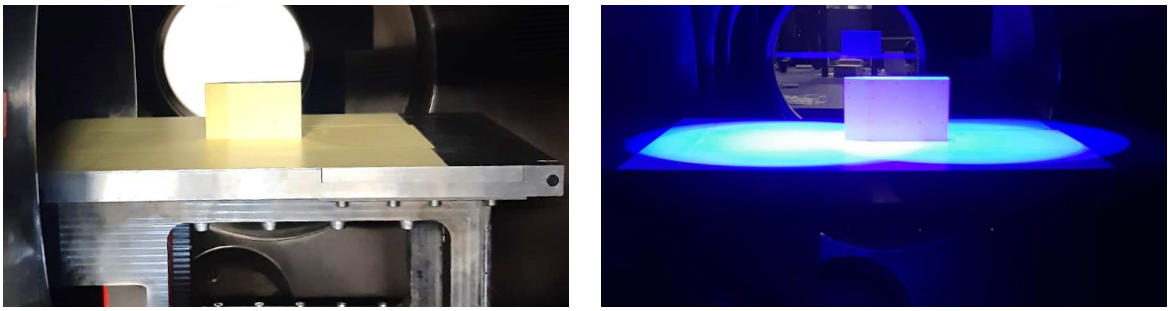

(a) Fin installed

(b) Fin with LED lighting

Figure 6: HEG test section

3.1 Zero deg AoF

Zero deg AoF experiments were conducted at both the XIII (1907 and 1908) and XV (1909) condition. Both runs, 1908 and 1909 were tripped using a granular trip, resulting in significant changes to the thermal loads on the flat plat incoming boundary layer and the SBLI caused by the fin. Top view heat flux distributions are shown in figure 7. The general structure is similar to the structure presented by Knight et al.[19] for turbulent supersonic flow around a sharp fin.

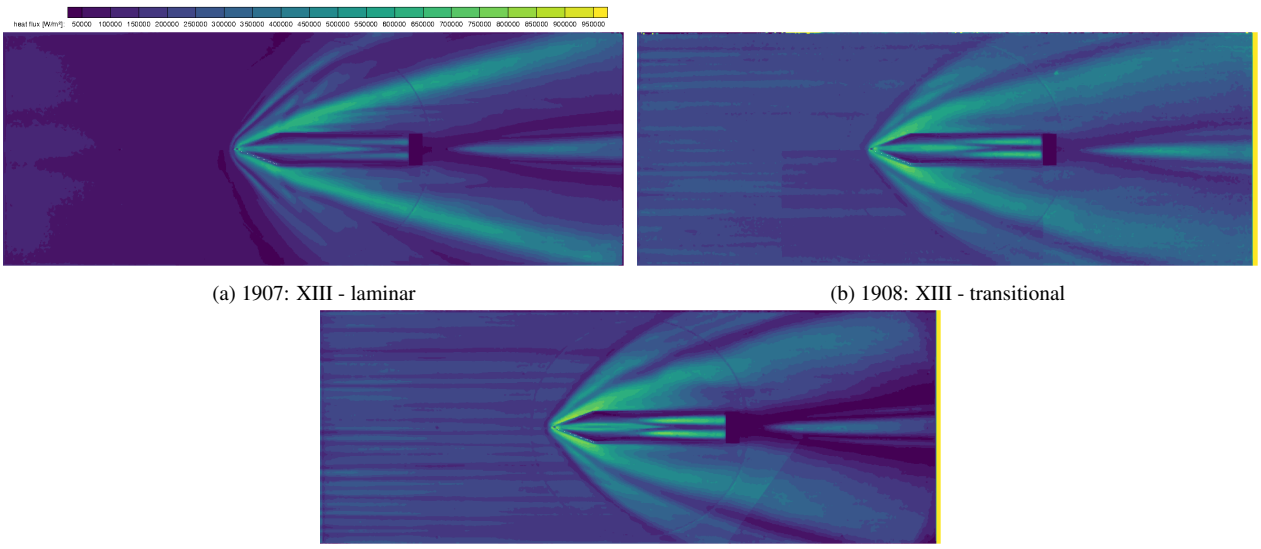

(a) 1907: XIII - laminar

(b) 1908: XIII - transitional

(c) 1909: XV - transitional

Figure 7: Experimental heat flux results for zero AoF for two different tunnel conditions.

Comparing condition XIII 1907 (laminar) and 1908 shows distinctive changes to the shock wave in front of the fin as well as the line of reattachment further downstream, indicating transitional/turbulent flow. This change is also visible in the heat flux in front of the fin from visible streak patterns for the tripped conditions. For both runs 1908 and 1909 noticeably higher heat fluxes are present especially in a small region near the fin leading edge.

The heat flux at three different transverse cuts (as defined in 4 is shown for all three runs. For these cuts the highest heat fluxes are attributed to the laminar case, even though globally the transitional runs show higher peaks near the fin LE.

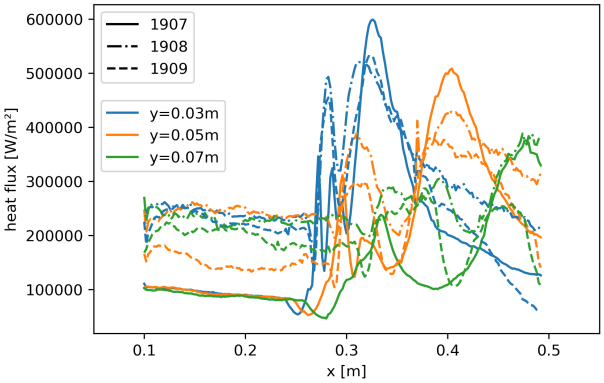

Figure 8: Experimental heat flux results for zero AoF for two different tunnel conditions at different transverse locations.

As shown in [4], the zero deg AoF experiments show very good symmetry on the stream wise cut planes. Similar results, albeit with a little more evident asymmetry in heat flux magnitude are shown for the transverse cuts at different stream wise locations shown in figure 9. In this visualization the increase in thermal loads over the laminar run is clearly visible for runs 1908 and 1909 for regions close to the fin.

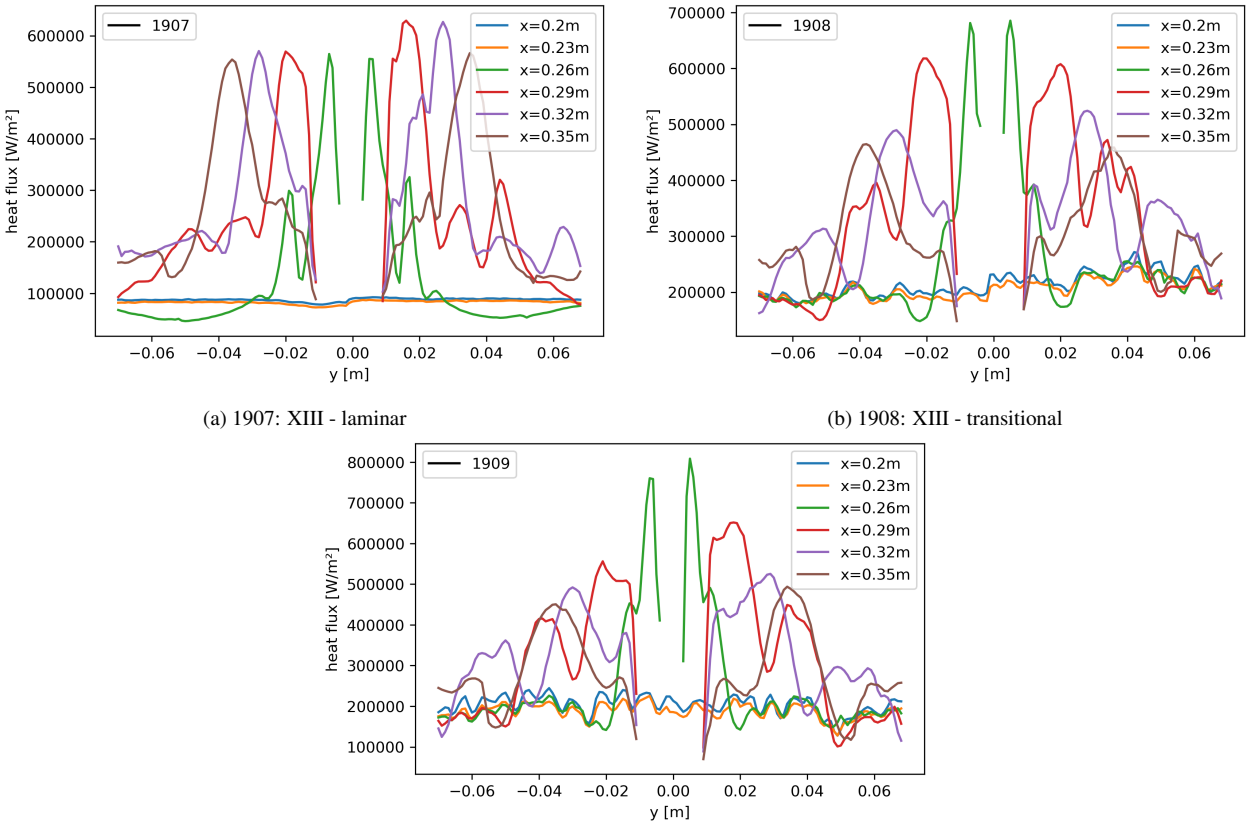

(a) 1907: XIII - laminar

(b) 1908: XIII - transitional

(c) 1909: XV - transitional

Figure 9: Experimental heat flux results for zero AoF for two different tunnel conditions at different stream wise locations.

3.2 15 deg AoF

15 deg AoF experiments were conducted for the XVII (1906), the XIII (1906 and 1912) and XV (1911) tunnel condition. Besides run 1906 all other runs were tripped using a granular trip, resulting in significant changes to the thermal loads on the flat plat incoming boundary layer and the SBLI caused by the fin, especially visible for the strong shock on the lower side of the plate (compare figure 10 and 11 bottom).

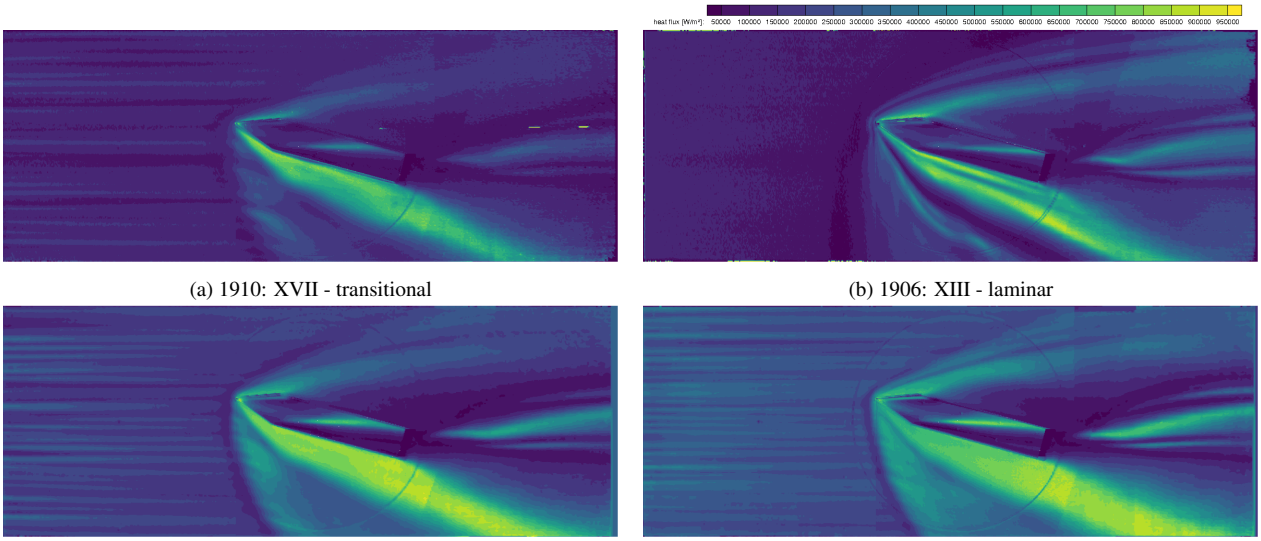

(a) 1910: XVII - transitional

(b) 1906: XIII - laminar

(c) 1912: XIII - transitional

(d) 1911: XV - transitional

Figure 10: Experimental heat flux results for 15 AoF for three different tunnel conditions.

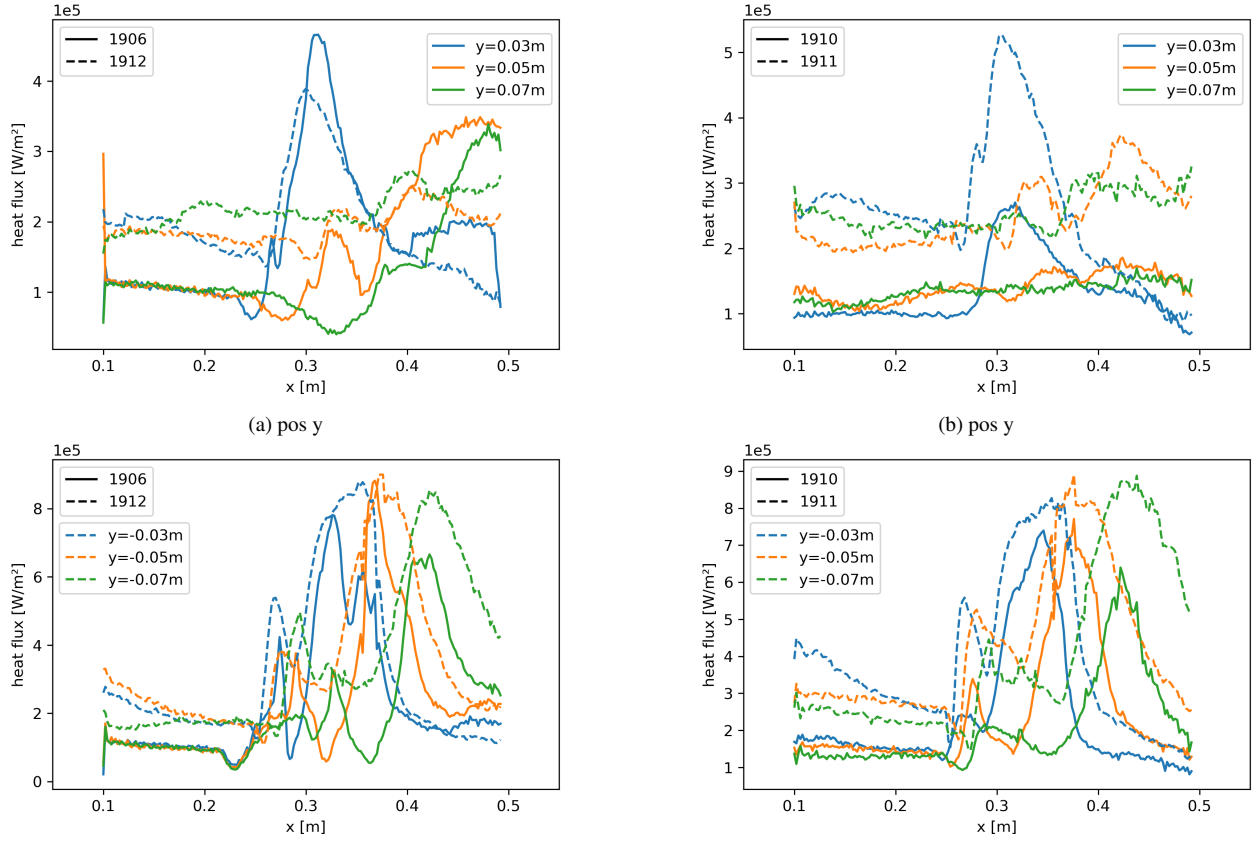

(a) pos y

(b) pos y

(c) neg y

(d) neg y

Figure 11: Experimental heat flux results for 15 AoF for three different tunnel conditions at different transverse locations.

4. CFD study

4.1 CFD code and boundary conditions

All numerical investigations in the framework of the present study were performed with the hybrid structured/unstructured DLR Navier-Stokes solver TAU[20], which is validated for a wide range of steady and unsteady sub-, trans- and hypersonic flow cases. The TAU code is a second order finite-volume solver for the Euler and Navier-Stokes equations in the integral form using eddy-viscosity, Reynolds-stress or detached- and large eddy simulation for turbulence modeling. The AUSMDV flux vector splitting scheme was applied together with MUSCL gradient reconstruction to achieve second order spatial accuracy.

4.1.1 Calculation matrix

The final calculation matrix is displayed in table 4. Asides from the laminar solver, both the Spalart-Allmaras (SA original)[21] and Menter k-ω SST[22] turbulence models were used. For some cases calculations using k-w Wilcox as well as the Wilcox implementation of the Reynolds Stress Modell (RSM)[23] were performed. Additionally one calculation for the same case using the hybrid RANS LES approach IDDES [24] was performed. IDDES is an improved zonal LES which has found more and more application in recent numerical scramjet (e.g [25]) studies. Lastly one XV case (1911) at 15 deg AoF was calculated using models for thermal and chemical non-equilibrium based on Gupta et al. [26] (11 species, 20 reactions) in combination with the Menter k-ω SST turbulence model. All other computations use thermodynamic data based on CEA for a thermally perfect air mixture.

Table 4: Calculation matrix

Cond.	AoF	laminar	SA	k-ω SST	k-ω Wilcox	RSM	IDDES (SA)
XIII	0 deg	+	+	+			
XIII	15 deg	+	+				
XV	0 deg	+	+	+	+		
XV	15 deg	+	+	+	+	+	+

4.1.2 Mesh

For the 3D study the plate and fin configuration are generated as a CAD model in ”free flight” configuration. This means no mounts or other wind tunnel hardware are present within the geometry. The mesh configuration is visualized in figure 12. The leading edge of fin and plate were meshed with a structured surface grid in order to obtain ideal boundary layer conditions.

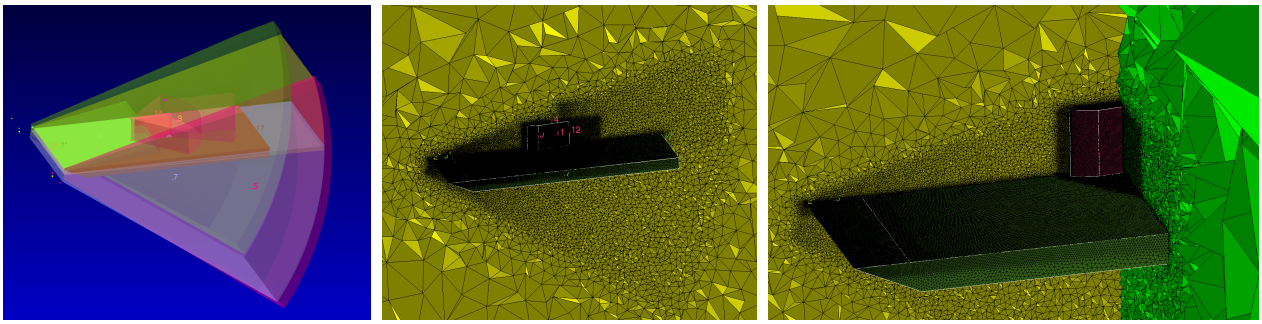

(a) CAD geometry and regions of refinement

(b) overview mesh

(c) mesh detail

Figure 12: Mesh generation.

Grid refinement volumes concentrate on the regions with shocks and expansions, as well as close to the regions of SBLI. Depending on AoF and case grid sizes between 8.5 and 12 Million points were generated. Comparisons on the influence of laminar flow /transition modeling / and different turbulence models for a 2D case were conducted and used to determine the best approach on the flat plate grid construction. The IDDES calculations were performed on the same grid.

5. Numerical results

5.1 Zero deg AoF

A comparison of all computed laminar and turbulent cases for the XIII condition and the XV condition in the top view of the plate is shown in figure 13 and 14 respectively.

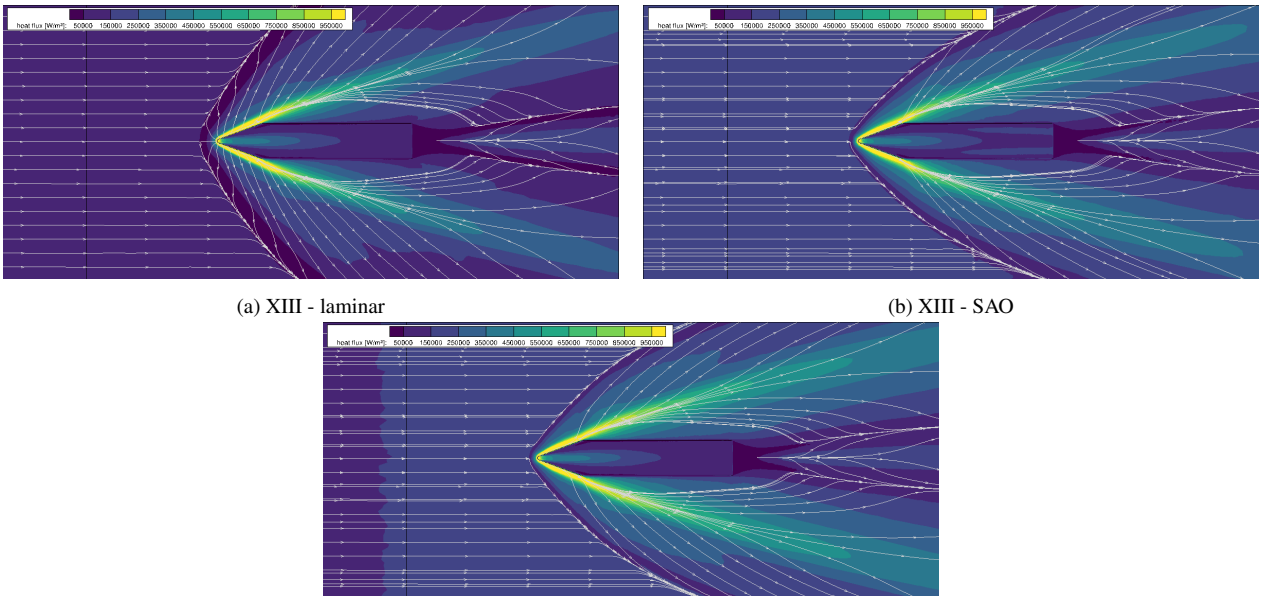

(a) XIII - laminar

(b) XIII - SAO

(c) XIII - k-ω SST

Figure 13: Numerical results for 0 deg AoF for conditions XIII and XV using different turbulence models. Streamlines on the surface represent shear stress vectors, surface colors show heat flux.

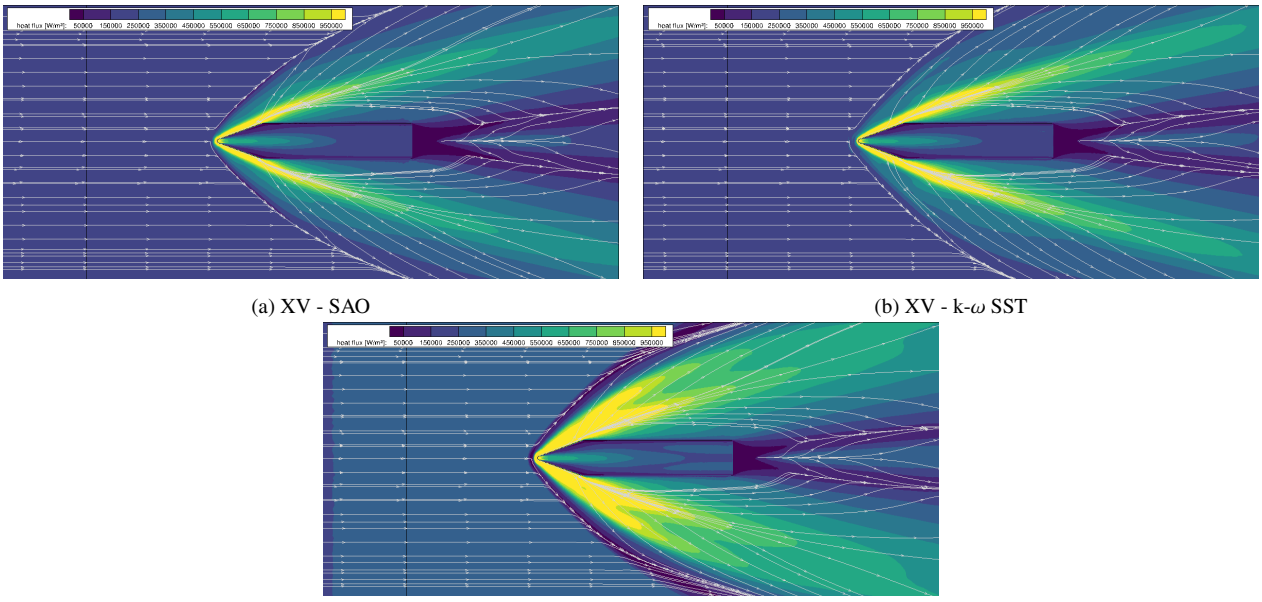

(a) XV - SAO

(b) XV - k-ω SST

(c) XV - k-ω Wilcox

Figure 14: Numerical results for 0 deg AoF for conditions XIII and XV using different turbulence models. Streamlines on the surface represent shear stress vectors, surface colors show heat flux.

5.2 15 deg AoF

A comparison of all computed laminar and turbulent cases for the XIII condition and the XV condition in the top view of the plate are shown in figure 15 and 16 respectively. As with the experiment results, clear differences are observable for the shape of the separation line between the laminar and turbulent cases for condition XIII.

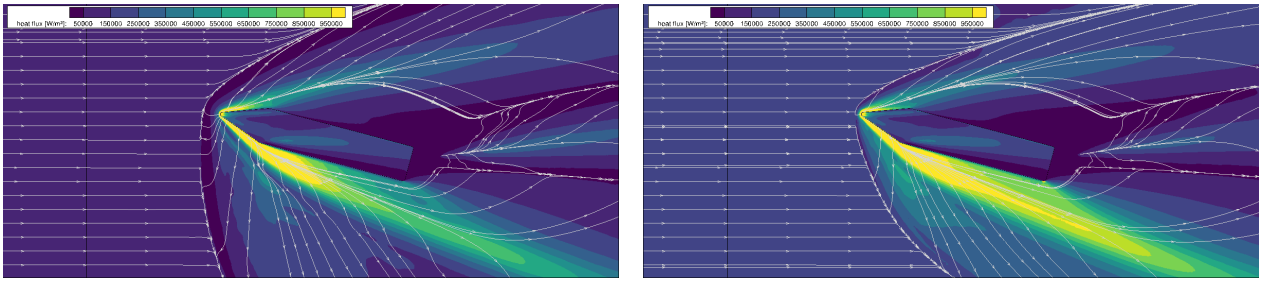

(a) XIII - laminar (b) XIII - SAO

Figure 15: Numerical results for 15 deg AoF for condition XIII: Comparison of laminar to turbulent case. Streamlines on the surface represent shear stress vectors, surface colors show heat flux.

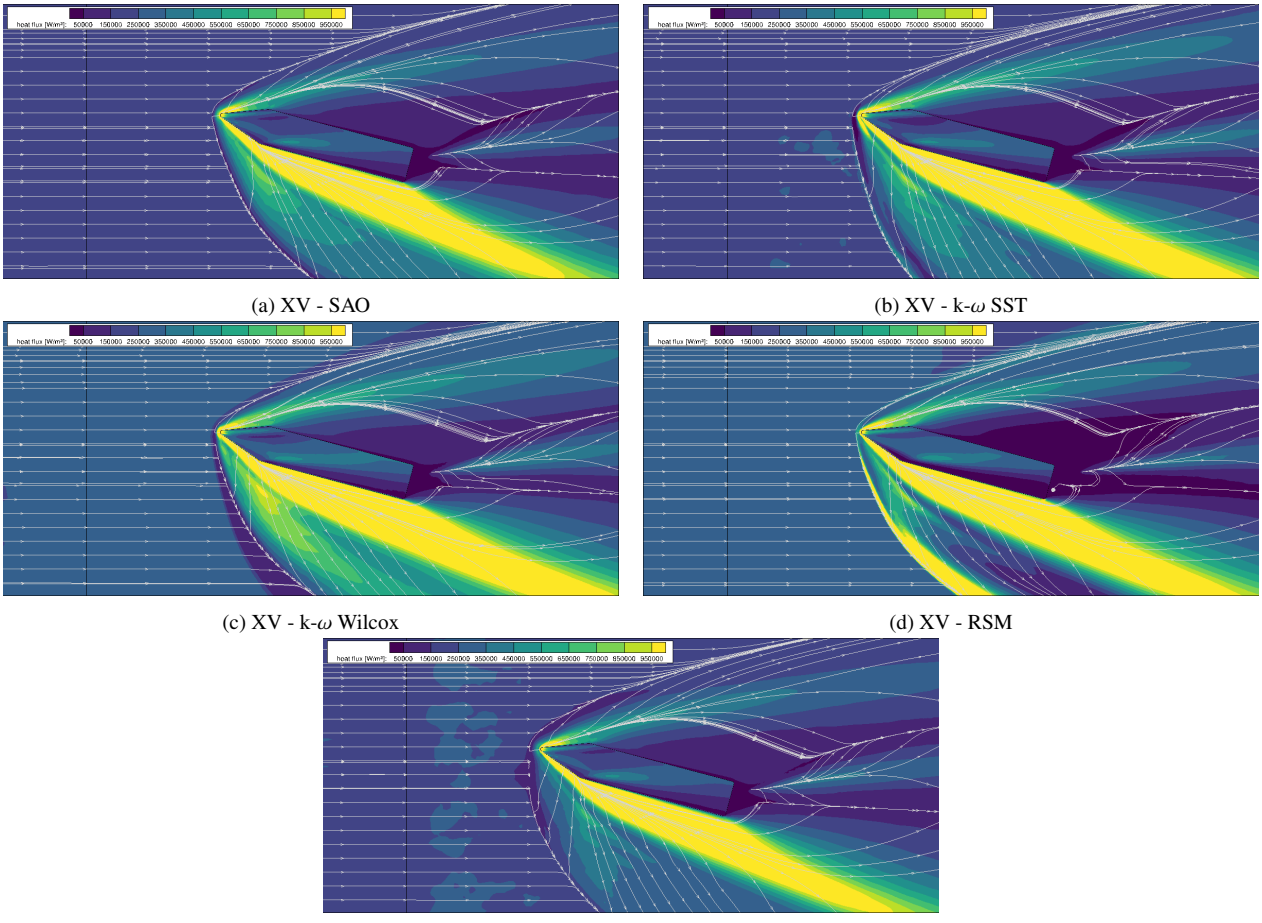

(a) XV - SAO

(b) XV - k-ω SST

(c) XV - k-ω Wilcox

(d) XV - RSM

(e) XV - IDDES/SA

Figure 16: Numerical results for 15 deg AoF for conditions XV (1911) using different turbulence models. Streamlines on the surface represent shear stress vectors, surface colors show heat flux.

The influence of thermal and chemical non equilibrium is investigated by using a three temperature model and the Gupta finite rate air chemistry model. The results in comparison to a thermally perfect gas are shown in figure 17. While the thermal loads distribution is generally similar, slight differences are seen in the heat flux near the separation

line of the large deflection angle (bottom) with are more discernible drop in heat flux magnitude and areas with higher heat flux magnitude further downstream.

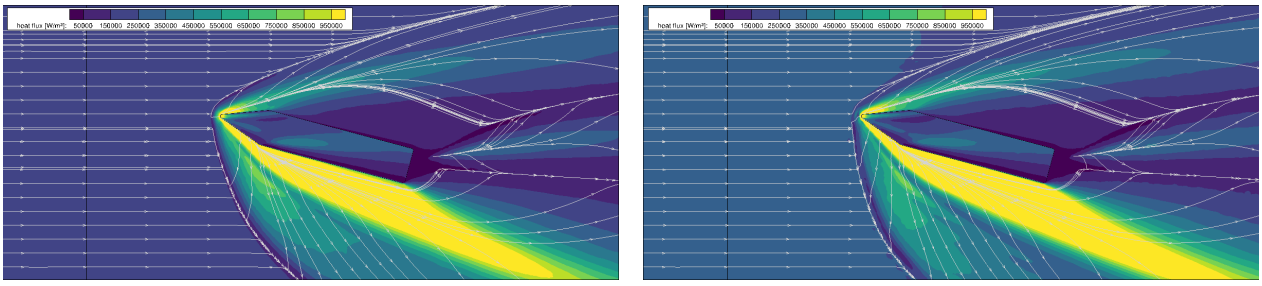

(a) XV - SAO

(b) XV - k-ω SST

Figure 17: Numerical results for 15 deg AoF for conditions XV (1911) using k-ω SST: non-equilibrium. Streamlines on the surface represent shear stress vectors, surface colors show heat flux.

6. Comparison between Experiment and CFD

For a more quantitative comparison between experiment and the CFD results the heat flux at different y locations is extracted for the runs for condition XIII and XV. The results of this extraction is shown in the following section. For the purpose of this evaluation, but also to smooth out some of the noise and uncertainty in positioning, the data is averaged over 50–100 pixels. The numerical data is interpolated on to the data locations from the experiment and averaged in the exact same way.

6.1 Zero deg AoF: Run 1907 and 1908

In our previous study[4] we have shown that for the location close to the centerline /close to the fin a y = 0.03 m, the experimental data and the numerical data (for the laminar run 1907, compare figure 18a) are a close match both in magnitude and gradients. For the locations further away the CFD underpredicts the heatflux magnitude but follows the general trend seen in the experiment. A possible cause could be SWBLI/separation induced transition which leads to higher heat flux downstream of the fin LE. This theory is supported by the data from run 1908 shown in figure 18b which matches fairly well with SA calculations, especially further away from the fin/centerline.

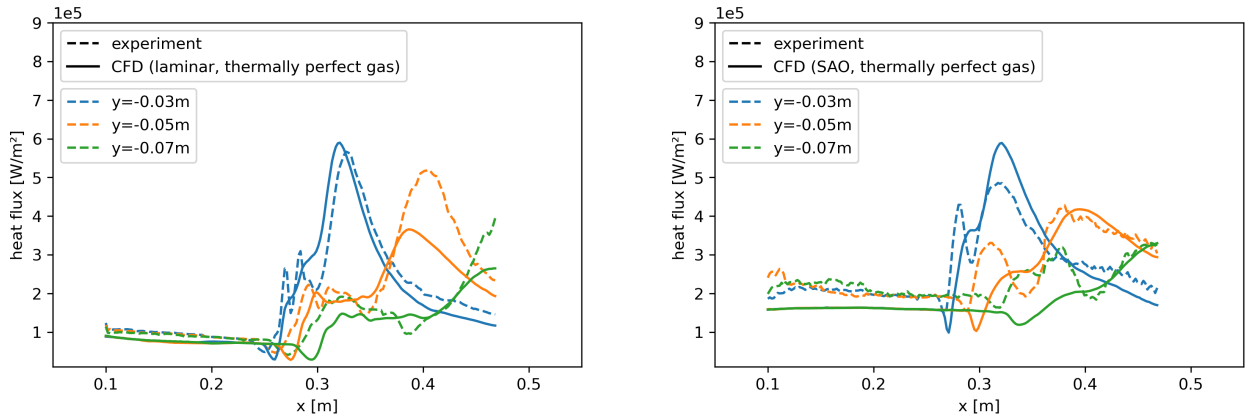

(a) XIII - laminar - 1907

(b) XIII - SA - 1908

Figure 18: Numerical results for zero deg AoF for conditions XIII (1907 and 1908).

6.2 Zero deg AoF: Run 1909

The comparison of experimental data and numerical data using the SAO and k-ω SST model for the high Re number case (XV) is shown in figure 19. Both numerical models predict significantly higher heat fluxes when compared to the experiment. Generally run 1909 appears to have low heat fluxes when compared to the flat heat flux before the SBLI which is can also be seen for the transverse cuts shown in figure 7c.

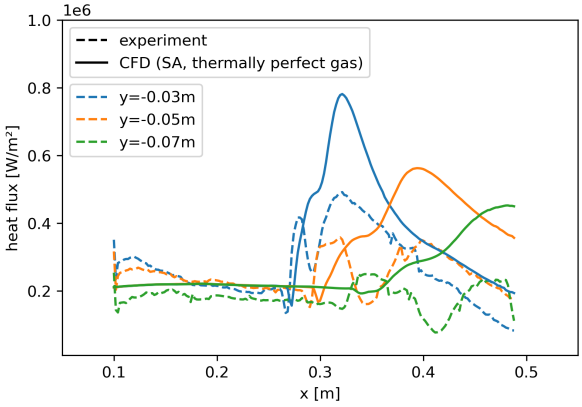

(a) XV - SA - 1909

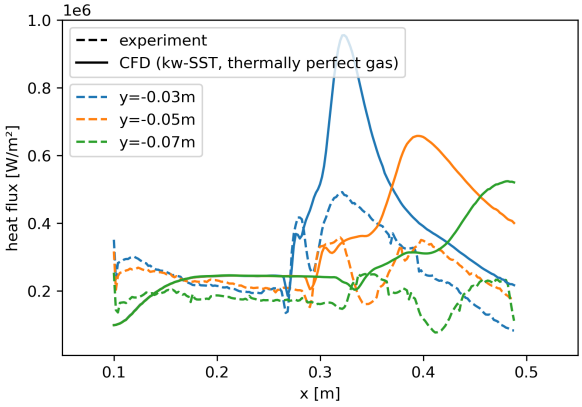

(b) XV - k-ω SST - 1909

Figure 19: Numerical results for zero deg AoF for conditions XV (1909).

6.3 15 deg AoF: Run 1906 and 1912

The comparison of runs 1906 and 1912 are shown in figure 20. Similar to the preceding XIII zero AoF cases, the agreement of experimental and results for runs 1906 and 1912 are quite good. Especially on the strong shock side (negative y) both the laminar and tripped/turbulent heat flux is predicted well in magnitude and position.

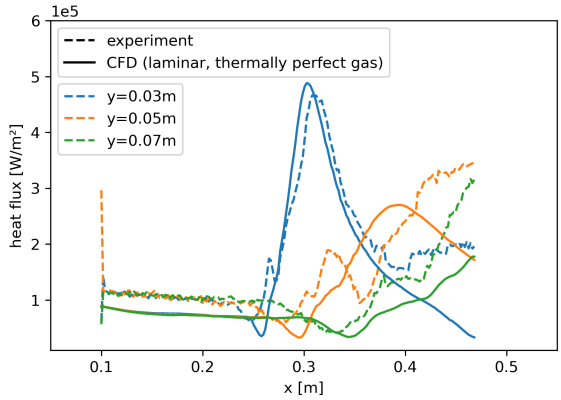

(a) XIII - laminar - 1906

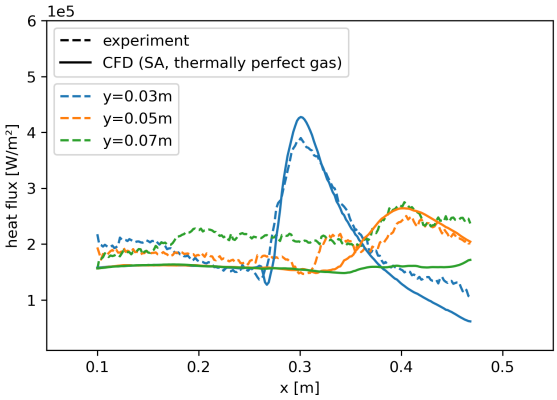

(b) XIII - SAO - 1912

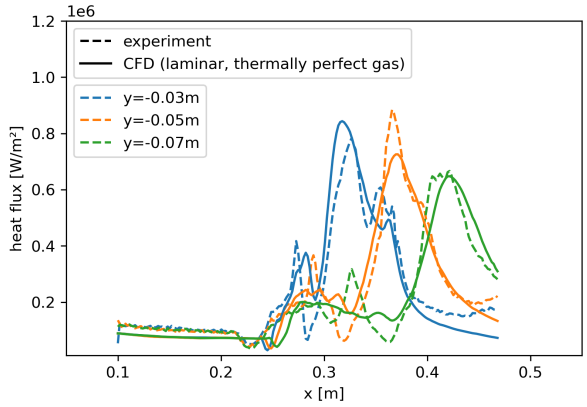

(c) XIII - laminar - 1906

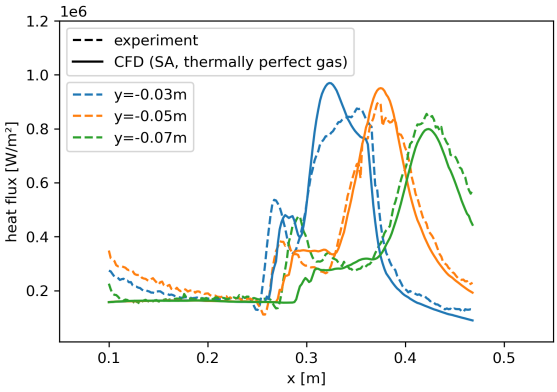

(d) XIII - SAO - 1912

Figure 20: Numerical results for 15 deg AoF for conditions XIII (1906 and 1912).

6.4 15 deg AoF: Run 1911

In the previous study[4] run 1911 was investigated and issues with lack of sensitivity (TSP paints emit lower signals at higher temperatures) were found resulting in ”saturation” at locations of high heat flux. Nevertheless the data is still valuable in the regions with lower thermal loads as the flow structure is still embedded in the recorded heat fluxes.

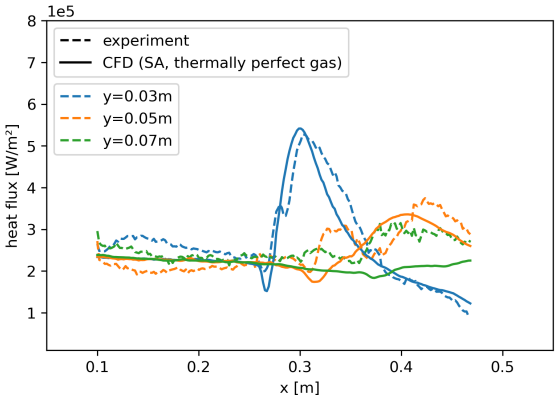

(a) XV - SAO

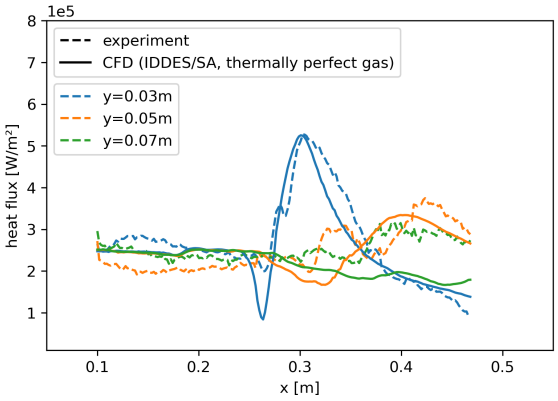

(b) XV - IDDES/SA

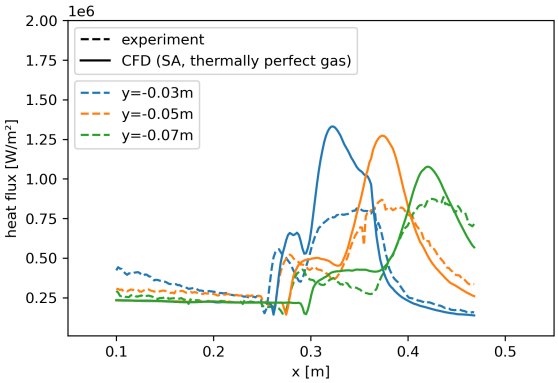

(c) XV - SAO

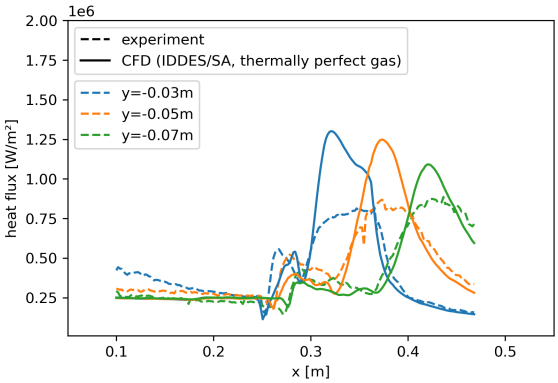

(d) XV - IDDES/SA

Figure 21: Numerical results for 15 deg AoF for conditions XV (1911) using SA and IDDES/SA

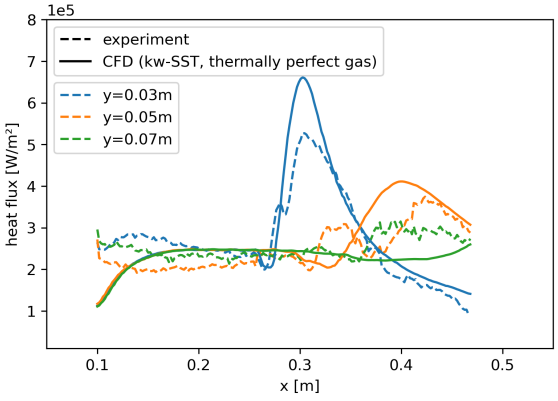

(a) XV - k-ω SST .

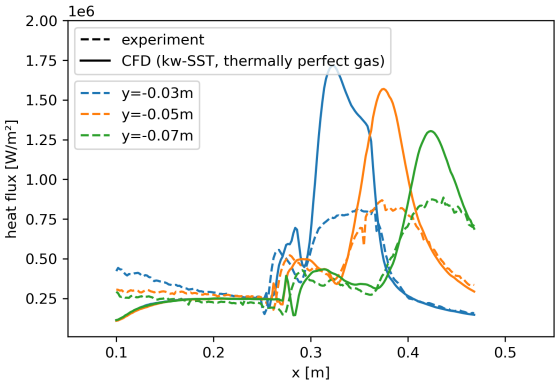

(b) XV - k-ω SST

Figure 22: Numerical results for 15 deg AoF for conditions XV (1911) kw-SST turbulence modelling for thermally perfect gas.

A comparison of the previously presented numerical data using the SA turbulence model with results from the IDDES approach are shown in figure 21. While there were some differences between the turbulence modelling approaches visible in 16, the differences on the streamwise cuts chosen for evaluation are quite minor as far as general

loads prediction magnitude and gradient is concerned. Minor improvements are made by the IDDES results with regards to the prediction of the location of the strong heat flux gradients on the negative (strong deflection) transverse locations especially for locations far away from the fin/centerline. For the positive transverse locations there appears an overprediction of the drop in heat flux by the IDDES, but both models predict the drop to be more exaggerated than the experiment. The same cuts are shown for the k-ω SST model in figure 22. Both the RSM model and the k-ω Wilcox performed poorly, in the case of the RSM model probably due to unpyhsically large production of k at the strong shock. Both cases are not shown due to space limitation.

The influence of thermal and chemical non-equilibrium effects were investigated by computations using the SAO and the k-ω SST turbulence model. A comparison is shown in figure 23. While the heat flux maximum magnitudes predicted by both approaches is similar (k-ω SST higher than the SA prediction), the non-equilibrium case using k-ω SST is spot on with both location and gradient of the regions with strong thermal loads. Only for the weak deflection side it performs as bad as the other models for the streamwise cuts far away from the centerline.

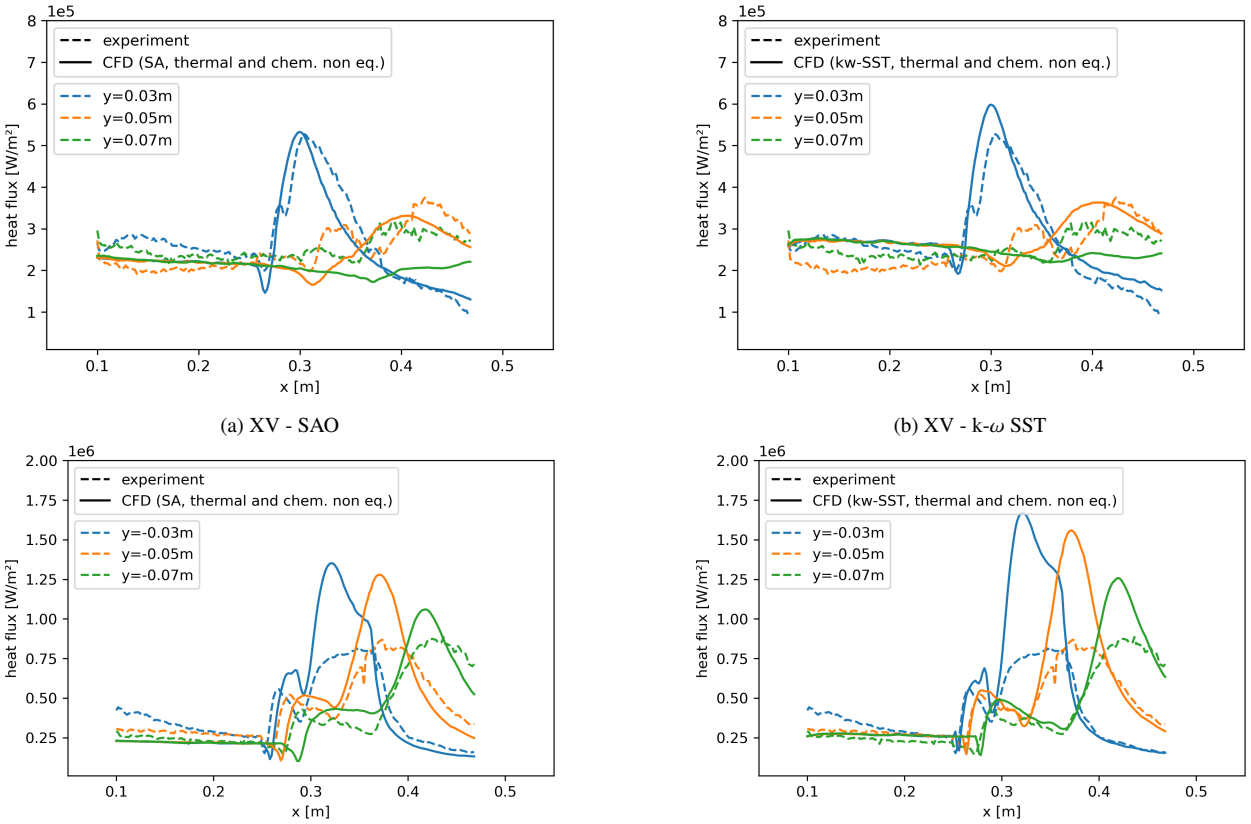

(a) XV - SAO

(b) XV - k-ω SST

(c) XV - SAO

(d) XV - k-ω SST

Figure 23: Numerical results for 15 deg AoF for conditions XV (1911) k-ω SST turbulence modelling for both thermally perfect gas and thermal and chemical non-equilibrium.

7. Conclusions

In this study the experimental and numerical work on laminar/transitional fin experiments in the HEG is described in detail. The object of investigation is a plate mounted fin which scales 1:2 to the fin flown in the STORT flight experiment. For the HEG experiment temperature sensitive paints were used to obtain distributed heat flux for SBLI on the plate for different fin angles, wind tunnel conditions and BL tripping approaches. Further numerical studies using the DLR TAU solver are used to interpret the physics of the hypersonic flow on the plate and around the fin. In the current study we extend the investigation to the other conditions/configurations studied and supplement the studies using RANS turbulence modelling by using Improved Detached eddy simulation(IDDES), as well as thermal and chemical non equilibrium for select cases in order to gain a better understanding of the complex flow field found in the experiment. Numerically two HEG freestream conditions are investigated using multiple turbulence models and fin angles. For four configurations (XIII: 0/15 deg AoF and XV: 0/15 deg AoF) comparisons between experimental

and CFD data were conducted. CFD calculations at the same conditions and configuration as investigated in the HEG were performed and compared for flow topology and turbulence model influence. While the low Re condition (XIII) is predicted fairly well with laminar and SA CFD calculations the high Re condition (XV) predictions are much more model dependent. Even though IDDES/SA shows some improvement over normal SA RANS modelling, the inclusion of thermal and chemical non-equilibrium together with k-ω-SST turbulence modelling lead to improvements with regards to gradient and location of the onset of strong thermal loads due to the SBLI.

References

[1] Joe D Watts. "Flight experience with shock impingement and interference heating on the X-15-2 research airplane". In: *NASA TM X-1669* (1968).

[2] Ali Gülhan, Sebastian Willems, and Florian Klingenberg. "STORT flight experiment for high speed technology demonstration". In: *72nd International Astronatical Congress*. international astronautical federation, Oct. 2021. URL: https://elib.dlr.de/147493/.

[3] Hiroshi Ozawa et al. "Fast-response temperature-sensitive-paint measurements on a hypersonic transition cone". In: *Experiments in Fluids* 56.1 (2015). Published online: 07. Dec. 2014, Article: 1853, pp. 1–13. URL: https://elib.dlr.de/93897/.

[4] Tobias Ecker et al. "Shockwave boundary layer interaction of laminar/transitional flow past a sharp fin". In: *2nd International Conference on High-Speed Vehicle Science & Technology HiSST 2022*. CEAS, Sept. 2022, pp. 1–13. URL: https://elib.dlr.de/188440/.

[5] John D. Schmisseur. "Hypersonics into the 21st century: A perspective on AFOSR-sponsored research in aerothermodynamics". In: *Progress in Aerospace Sciences* 72 (2015). Celebrating 60 Years of the Air Force Office of Scientific Research (AFOSR): A Review of Hypersonic Aerothermodynamics, pp. 3–16. ISSN: 0376-0421. DOI: https://doi.org/10.1016/j.paerosci.2014.09.009. URL: https://www.sciencedirect.com/science/article/pii/S0376042114000980.

[6] Ali Gülhan et al. "Projekt STORT-Schlüsseltechnologien für hochenergetische Rückkehrflüge der Trägerstufen". Dec. 2022. URL: https://elib.dlr.de/193289/.

[7] Thomas Reimer et al. "Design, Manufacturing and Assembly of the STORT Hypersonic Flight Experiment Thermal Protection System". In: *25th AIAA International Space Planes and Hypersonic Systems and Technologies Conference*. Ed. by American Institute of Aeronautics and Astronautics. May 2023. URL: https://elib.dlr.de/195465/.

[8] Rainer Kirchhartz and Wolfgang Jung. "MORABA Activities in Retrospect: New Flight Test Capabilities & Competences". In: *24th ESA Symposium on European Rocket & Balloon programmes and related research*. 2019. URL: https://elib.dlr.de/131945/.

[9] H. Ozawa et al. "Fast response temperature sensitive paint measurements on a hypersonic transition cone". In: *Experiments in Fluids* 56 (2014), p. 1853. DOI: 10.1007/s00348-014-1853-y.

[10] J. Martinez Schramm et al. "Development of Temperature Sensitive Paints in the High Enthalpy Shock Tunnel Göttingen, HEG". In: *8th European Symposium on Aerothermodynamics for Space Vehicles*. 2015.

[11] Michael C. Adler and Datta V. Gaitonde. "Influence of separation structure on the dynamics of shock/turbulent-boundary-layer interactions". In: *Theoretical and Computational Fluid Dynamics* 36.2 (Apr. 2022), pp. 303–326. ISSN: 1432-2250. DOI: 10.1007/s00162-021-00590-y. URL: https://doi.org/10.1007/s00162-021-00590-y.

[12] J. D. Pickles et al. "On the mean structure of sharp-fin-induced shock wave/turbulent boundary layer interactions over a cylindrical surface". In: *Journal of Fluid Mechanics* 865 (2019), pp. 212–246. DOI: 10.1017/jfm.2019.53.

[13] James A. Threadgill et al. "Fin-induced Shock Boundary Layer Interactions on a Flat Plate and Hollow Cylinder at Mach 5". In: *AIAA SCITECH 2022 Forum*. DOI: 10.2514/6.2022-1816. URL: https://arc.aiaa.org/doi/abs/10.2514/6.2022-1816.

[14] Sathyan Padmanabhan et al. "Laminar/Transitional Fin-induced Shock Wave Boundary-Layer Interactions at Mach 5". In: *AIAA SCITECH 2023 Forum*. DOI: 10.2514/6.2023-1234. URL: https://arc.aiaa.org/doi/abs/10.2514/6.2023-1234.

[15] N.T Smith et al. “Use of Temperature Sensitive Paint in the AEDC Hypervelocity Wind Tunnel 9”. In: *12th AIAA International Space Planes and Hypersonic Systems and Technologies*. DOI: 10.2514/6.2003-6962. eprint: https://arc.aiaa.org/doi/pdf/10.2514/6.2003-6962. URL: https://arc.aiaa.org/doi/abs/10.2514/6.2003-6962.

[16] Klaus Hannemann et al. “The High Enthalpy Shock Tunnel Göttingen of the German Aerospace Center (DLR)”. In: *Journal of large-scale research facilities JLSRF* 4 (2018), p. 133.

[17] W. J. Cook J. C. and E. J. Felderman. “Reduction of data from thin-film heat-transfer gages - A concise numerical technique.” In: *AIAA Journal* 4.3 (1966), pp. 561–562. ISSN: 0001-1452. DOI: 10.2514/3.3486. URL: http://dx.doi.org/10.2514/3.3486.

[18] Divek Surujhlal et al. “Hypersonic Boundary-Layer Transition on Cold-Wall Canonical Geometries with Quantified Distributed Roughness Elements”. In: *AIAA Journal* 61.2 (2023), pp. 543–554. DOI: 10.2514/1.J062131.

[19] Doyle D. Knight et al. “Structure of supersonic turbulent flow past a sharp fin”. In: *AIAA Journal* 25.10 (1987), pp. 1331–1337. DOI: 10.2514/3.9787. eprint: https://doi.org/10.2514/3.9787. URL: https://doi.org/10.2514/3.9787.

[20] S. Langer, A. Schwöppe, and N. Kroll. “The DLR Flow Solver TAU – Status and Recent Algorithmic Developments”. In: *AIAA Paper AIAA-2014-0080*. 52nd Aerospace Sciences Meeting (2014). DOI: 10.2514/6.2014-0080.

[21] Spalart, P.R. and Allmaras, S.R. “A One-Equation Turbulence Model for Aerodynamic Flows”. In: *AIAA Paper AIAA-92-0439* (1992). DOI: 10.2514/6.1992-439.

[22] F. R. Menter. “Two-equation eddy-viscosity turbulence models for engineering applications”. In: *AIAA Journal* 32.8 (1994), pp. 1598–1605. DOI: 10.2514/3.12149.

[23] David Wilcox. *Turbulence Modeling for CFD (Third Edition) (Hardcover)*. Jan. 2006.

[24] Mikhail L. Shur et al. “A hybrid RANS-LES approach with delayed-DES and wall-modelled LES capabilities”. In: *International Journal of Heat and Fluid Flow* 29.6 (2008), pp. 1638–1649. ISSN: 0142-727X. DOI: https://doi.org/10.1016/j.ijheatfluidflow.2008.07.001. URL: https://www.sciencedirect.com/science/article/pii/S0142727X08001203.

[25] Wei Yao et al. “Performance analysis of a strut-aided hypersonic scramjet by full-scale IDDES modeling”. In: *Aerospace Science and Technology* 117 (2021), p. 106941. ISSN: 1270-9638. DOI: https://doi.org/10.1016/j.ast.2021.106941. URL: https://www.sciencedirect.com/science/article/pii/S127096382100451X.

[26] Roop Narayan Gupta, Jerrold M. Yos, and Richard A. Thompson. “A review of reaction rates and thermodynamic and transport properties for the 11-species air model for chemical and thermal nonequilibrium calculations to 30000 K”. In: 1989.